



Exploration of sea anemone-inspired high-performance biomaterials with enhanced antioxidant activity

Lulu Wang^{a,b}, Xiaokang Zhang^{a,b}, Pingping Xu^{a,b}, Jicheng Yan^{a,b}, Yuzhong Zhang^{a,b,c}, Hainan Su^c, Chengjun Sun^{b,d}, Qiang Lu^{e,*}, Weizhi Liu^{a,b,*}

^a Sars-Fang Centre, MOE Key Laboratory of Marine Genetics and Breeding, College of Marine Life Sciences, Ocean University of China, Qingdao, 266003, China

^b Laboratory for Marine Biology and Biotechnology, Pilot National Laboratory for Marine Science and Technology, Qingdao, 266071, China

^c State Key Laboratory of Microbial Technology, Marine Biotechnology Research Center, Shandong University, Qingdao, 266237, China

^d Key Laboratory of Marine Eco-environmental Science and Technology, Marine Bioresource and Environment Research Center, First Institute of Oceanography, Ministry of Natural Resources (MNR), Qingdao, 266061, China

^e National Engineering Laboratory for Modern Silk, Collaborative Innovation Center of Suzhou Nano Science and Technology, Soochow University, Suzhou, 215123, China

ARTICLE INFO

Keywords:

Sessile marine organisms
Antioxidant biomaterials
Water-resistant coatings
Redox-responsive hydrogels
Photoaging

ABSTRACT

Antioxidant biomaterials have attracted much attention in various biomedical fields because of their effective inhibition and elimination of reactive oxygen species (ROS) in pathological tissues. However, the difficulty in ensuring biocompatibility, biodegradability and bioavailability of antioxidant materials has limited their further development. Novel bioavailable antioxidant materials that are derived from natural resources are urgently needed. Here, an integrated multi-omics method was applied to fabricate antioxidant biomaterials. A key cysteine-rich thrombospondin-1 type I repeat-like (TSRL) protein was efficiently discovered from among 1262 adhesive components and then used to create a recombinant protein with a yield of 500 mg L⁻¹. The biocompatible TSRL protein was able to self-assemble into either a water-resistant coating through Ca²⁺-mediated coordination or redox-responsive hydrogels with tunable physical properties. The TSRL-based hydrogels showed stronger 1,1-diphenyl-2-picrylhydrazyl (DPPH) radical scavenging rates than glutathione (GSH) and ascorbic acid (Aa) and protected cells against external oxidative stress significantly more effectively. When topically applied to mice skin, TSRL alleviated epidermal hyperplasia and suppressed the degradation of collagen and elastic fibers caused by ultraviolet radiation B (UVB) irradiation, confirming that it enhanced antioxidant activity *in vivo*. This is the first study to successfully characterize natural antioxidant biomaterials created from marine invertebrate adhesives, and the findings indicate the excellent prospects of these biomaterials for great applications in tissue regeneration and cosmeceuticals.

1. Introduction

Antioxidant biomaterials have been used in antitumor drug delivery [1], soft tissue regeneration [2], chronic wound healing [3] and cosmeceutical applications [4]. Sustained inflammatory responses in tissues and wounds usually cause accumulation of reactive oxygen species (ROS), resulting in abnormal cell growth, a disordered immune response, and slow wound healing [5]. Antioxidants can eliminate

harmful excess ROS to inhibit or delay molecular oxidation. Biomaterials with antioxidant activity are essential for regenerating tissues since they can remove ROS rapidly and continuously from damaged tissues [6]. Recently, antioxidant hydrogel dressings were found to be remarkably beneficial for wound healing. For example, an injectable hydrogel with antioxidant activity was prepared via introduction of gallic acid-conjugated gelatin into gelatin-hydroxyphenyl propionic hydrogels; the resulted hydrogel accelerated chronic wound healing and

Peer review under responsibility of KeAi Communications Co., Ltd.

* Corresponding author. MOE Key Laboratory of Marine Genetics and Breeding, College of Marine Life Sciences, Ocean University of China, Qingdao, 266003, China.

** Corresponding author. National Engineering Laboratory for Modern Silk, Collaborative Innovation Center of Suzhou Nano Science and Technology, Soochow University, Suzhou, 215123, China.

E-mail addresses: lvqiang78@suda.edu.cn (Q. Lu), liuweizhi@ouc.edu.cn (W. Liu).

<https://doi.org/10.1016/j.bioactmat.2021.08.021>

Received 14 June 2021; Received in revised form 9 August 2021; Accepted 18 August 2021

Available online 4 September 2021

2452-199X/© 2021 The Authors. Publishing services by Elsevier B.V. on behalf of KeAi Communications Co. Ltd. This is an open access article under the CC

BY-NC-ND license (<http://creativecommons.org/licenses/by-nc-nd/4.0/>).

promoted hair follicle formation [7].

Antioxidant and self-antioxidant materials are often introduced into various biomaterials to endow them with antioxidant capacity. Many loaded antioxidant components are released too quickly, are released incompletely or are unstable during the release process [3]. Therefore, designing self-antioxidant biomaterials through chemical modifications and genetic engineering is a desirable strategy. Functional groups sensitive to superoxide and hydrogen peroxide, such as polythioketal and polypropylene sulfide, have been grafted into synthetic polymer frameworks to scavenge free radicals and resist oxidative stress [8]. However, the low bioavailability and inferior scale-up production of modified biomaterials limit their application [8]. Thus, exploration of bioavailable antioxidant biomaterials derived from natural resources is urgently needed. Numerous high-value biomaterials originating from marine organisms have been found in the last decade [9]. Sessile marine organisms live in seawater with saturating levels of dissolved oxygen at pH ~8. To maintain redox balance, adhesive plaques on these organisms utilize reducing proteins for protection against adverse oxidation [10, 11]. Many antioxidant proteins must be present at the interface with the substratum. For example, mussels secrete cysteine-rich mfp-6 to the distal depression of the foot during plaque deposition [12,13]. Therefore, marine adhesives might be unexplored resources for antioxidant biomaterials.

Omics technologies have significantly contributed to the understanding of underwater bioadhesion and have provided a number of putative protein-based biomaterials [14]. The adhesive proteins of sessile marine organisms with a defined secretory gland, such as mussels and scallops, can be identified through a combination of transcriptomics and proteomics [15,16]. However, distinguishing the boundary of the secretory gland remains difficult in some species that adhere to substrates by secreting mucus/cements; contamination inevitably occurs during the harvest of adhesive components from organisms such as sea stars [17], limpets [18], and ascidians [19] (Fig. 1). The large numbers of protein sequences in omics libraries make it impossible to effectively identify biomaterials with the desired functions.

Sea anemones are typical sessile marine invertebrates that live in

intertidal zones. Sea anemones secrete adhesives from their pedal discs to firmly adhere to the substratum [20]. In this study, we applied combined omics to efficiently discover and produce an antioxidant protein. We found that the cysteine-rich thrombospondin-1 type I repeat-like (TSRL) protein not only fabricated a coating with Ca²⁺-mediated wet-resistance, but also self-assembled into hydrogels with tunable physical properties. Both the novel coating and the hydrogels exhibited beneficial antioxidative activity. Our results suggested that the TSRL-based hydrogels were able to resist oxidative stress damage *in vivo* and *in vitro*. This study facilitates the future discovery of novel functional biomaterials from previously unexplored sessile marine organisms, which might fill the gap between biology and biomimetic materials (Fig. 1).

2. Materials and methods

2.1. Dynamic light scattering (DLS)

TSRL protein solutions were diluted in 20 mM Tris-HCl (pH 8.5) to 1 mg mL⁻¹ and passed through 0.22 μm syringe filters. The samples were introduced into quartz cuvettes and stabilized at 25 °C. The hydrodynamic size of the protein was measured on a DLS analyzer (Malvern Zetasizer Nano ZS, Worcestershire, UK). Intensity distribution data were collected from three biological replicates.

2.2. Metal ion-induced protein aggregation

The purified TSRL protein was diluted to 1 mg mL⁻¹ with 20 mM Tris-HCl (pH 8.5). 50 μL of Ca²⁺ at a final concentration of 10 mM was added to 50 μL of the protein solutions. The resulting aggregates were quickly transferred to glass slides, allowed to deposit for 15 min at room temperature, and then washed thoroughly with deionized water. The adsorbed proteins were visualized using Coomassie blue staining. The surfaces were observed by using a MoticAE2000 microscope. Additionally, 0.5 mM metal ions were added to the TSRL protein for 30 min. Turbidity changes during the gelation process were monitored at 340

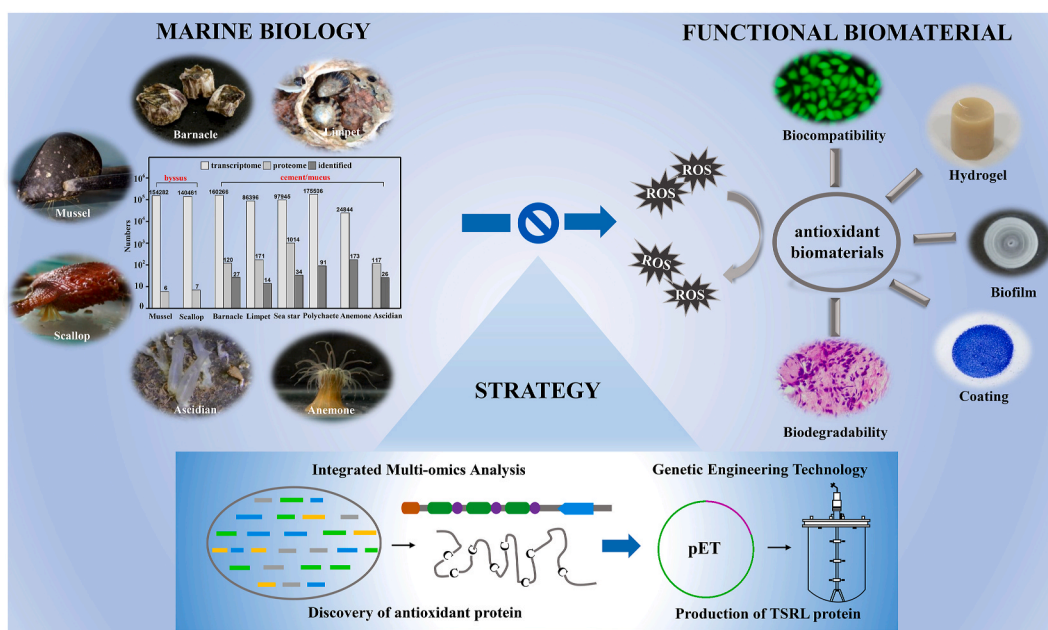


Fig. 1. Design of bioinspired antioxidant biomaterials from sessile marine organisms. The adhesive plaques of sessile marine organisms usually contain reducing proteins to shield against adverse oxidation in seawater at pH~8. Abundant adhesive proteins have been identified through transcriptomics and proteomics in sessile marine organisms such as mussels, scallops, barnacles, and limpets, but it is not possible to directly screen antioxidant proteins. In our strategy, multi-omics and sequence analysis were combined to efficiently identify antioxidant peptides, and genetic engineering technology was further applied for large-scale protein production.

nm using a microplate reader (Synergy H1, BioTek, USA) in absorbance mode.

2.3. Evaluation of adsorption ability

Aluminum, polystyrene, and glass plates were used as substrates for surface coating analysis. Mixtures of TSRL or Human TSR (Protein Data Bank: 3R6B) proteins and Ca^{2+} were deposited on the substrates for 15 min. The prepared surfaces were shaken in an aqueous environment for 1 h and 48 h at 25 °C to assess stability and water resistance. The adsorbed proteins were then visualized using Coomassie blue staining. The individual TSRL protein solutions were also deposited on the substrates and used as negative controls.

2.4. Formation of the hydrogel

The purified TSRL protein was dialyzed into 20 mM Tris-HCl (pH 8.5) at a concentration of 1 mg mL⁻¹. The protein was concentrated to 70 mg mL⁻¹ with an ultrafiltration tube. The high-concentration TSRL protein solution was transferred into different molds and stored for 3 days at 15 °C to form highly flexible hydrogels. Additionally, 0.03% hydrogen peroxide (H_2O_2)/10 mM dithiothreitol (DTT) was introduced to the TSRL protein solution to prepare redox-treated hydrogels.

2.5. Analysis of gelation kinetics

A total of 200 μL of TSRL protein solution (30, 50 or 70 mg mL⁻¹) was placed into each well of covered 96-well plates at 15 °C. Turbidity changes during the gelation process were monitored at 570 nm using a microplate reader in absorbance mode. Each experiment was performed five times, and the data are presented as the mean values.

2.6. Scanning electron microscopy (SEM)

A coating with a diameter of 1 cm was formed on a cover glass. The coating was washed with deionized water and then air-dried. The cylindrical hydrogels were prepared with a diameter of 5 mm and a height of 2 mm. The hydrogels were flash frozen in liquid nitrogen and immediately freeze-dried. The prepared materials were sputter-coated with platinum in an ion sputter coater (Hitachi MC1000). The thickness of the sputtered layer created by sputtering at a current of 15 mA for 45 s was approximately 8 nm. SEM (Hitachi S-3400 N, 15 kV) was used to observe the surface morphology of the TSRL-based coating and hydrogels.

2.7. Atomic force microscopy (AFM)

The protein solutions were cast on freshly cleaved mica surfaces at room temperature and allowed to dry for 24 h. AFM was performed in tapping mode using a Nanowizard I atomic force microscope (JPK Instruments, Berlin, Germany). The scan rate was maintained at 1 Hz. Images were collected with a scanning window of 2 μm and analyzed using Nanoscope Analysis 1.5 software.

2.8. Mechanical tests

Compressive testing of the protein hydrogels was carried out using an electronic universal testing machine (Exceed E42.503 MTS Products, Minnesota, USA) with a load cell of 50 N at 25 °C. Cylindrical hydrogels with a diameter of 10 mm and an initial thickness of 10 mm were placed on a metal plate. The compression rate was 2 mm min⁻¹, and the linear regions of the stress-strain curve were taken to calculate the compressive modulus.

2.9. Fourier transform infrared spectroscopy (FTIR)

FTIR was carried out on a Spotlight 200i FTIR Microscope System (PerkinElmer, US). Samples were quickly frozen in liquid nitrogen and then lyophilized for 24 h. All spectra were recorded with a resolution of 2 cm⁻¹, and the wavenumbers ranged from 500 to 4000 cm⁻¹.

2.10. In vitro enzymatic degradation

To test the enzymatic degradation of the hydrogels, native and H_2O_2 -treated hydrogels were prepared, and the original hydrogel mass was determined (W_0). Protease XIV derived from *Streptomyces griseus* was prepared at a concentration of 0.2 U mL⁻¹ by dissolving the enzyme in sterile PBS. The hydrogels were immersed in 3.5 mL of protease solution or PBS solution at 37 °C. The enzyme solutions were changed every 24 h. After removing the buffer from the surfaces of the hydrogels, the hydrogels were weighed again (W_t). The degradation ratios of the hydrogels were calculated using Equation (1):

$$\text{Degradation ratio (\%)} = \frac{W_0 - W_t}{W_0} \times 100. \quad (1)$$

To study the influence of the redox environment on the degradation behavior of the hydrogels, 0.03% H_2O_2 /10 mM DTT was added to the PBS solution, and the degradation rates of the hydrogels were calculated at a predetermined time point.

2.11. Cytocompatibility analysis

L929 cells were used to evaluate the cytotoxicity of the biomaterials by the 3-(4,5-dimethylthiazol-2-yl)-2,5-diphenyltetrazolium bromide (MTT) colorimetry. TSRL protein/coatings/hydrogels formed in 24-well plates were disinfected with ultraviolet light. The cells (1×10^5 cells mL⁻¹) were seeded on the samples and cultured at 37 °C under 5% CO_2 for 24, 48 or 72 h. MTT was added to the cells, and the cells were incubated for 4 h. The absorbance was measured at 490 nm ($n = 4$), and A_{control} was defined as 100%. Cell viability was calculated using Equation (2):

$$\text{Cell viability (\%)} = \frac{A_{\text{sample}}}{A_{\text{control}}} \times 100. \quad (2)$$

Live/dead cell staining was used to assess the cell state. The concentrations of calcein-AM (live cells, green color) and propidium iodide (PI, dead cells, red color) were 2 mM and 4.5 μM , respectively, and 200 μL of this mixture solution was added to each well. Actin-Tracker Green was used to observe cell morphology. Images were obtained using a Nikon Eclipse Ti microscope (Nikon Corporation, Tokyo, Japan).

2.12. In vitro antioxidant experiments

Antioxidant activity was quantified using the 1,1-diphenyl-2-picrylhydrazyl (DPPH) radical scavenging method. To determine the antioxidant activity of the TSRL protein solutions, 100 μL samples at various concentrations (2–40 μM) were added to 100 μL of DPPH solution (0.2 mM) in 96-well microplates and left in the dark for 30 min. Glutathione (GSH) and ascorbic acid (Aa) (25 μM) were used as positive controls. To determine the antioxidant activity of the coatings, a mixture of 90 μL of protein solution and 10 μL of Ca^{2+} was added to 100 μL of DPPH radical solution. To determine the antioxidant activity of the hydrogels, a reaction mixture consisting of 1.0 mL of hydrogel and 3.0 mL of the DPPH radical solution was prepared. The absorbance was measured using a microplate reader at 517 nm ($n = 4$). The free radical scavenging effect was calculated using Equation (3):

$$\text{Scavenging effect (\%)} = \left(1 - \frac{A_{\text{sample}}}{A_{\text{DPPH}}}\right) \times 100. \quad (3)$$

2.13. Intracellular antioxidant determination

The hydrogels and L929 cells were cocultured for 24 h in 24-well plates with 1 mL of fresh Dulbecco's modified Eagle medium (DMEM). Then, 0.15 or 0.3 mM H₂O₂ was added to the culture medium for 12 h of incubation in a 37 °C incubator. Total cellular ROS levels were determined using ROS assay kits (Beyotime Institute of Biotechnology, Shanghai, China). The fluorescence of 2,7-dichlorodihydrofluorescein diacetate (DCFH-DA) was measured at an excitation wavelength of 488 nm and an emission wavelength of 525 nm.

2.14. In vivo antioxidant experiments

Male C57BL/6J mice (6 weeks old) were purchased from Pengyue Experimental Animal Breeding Co., Ltd. (Jinan, China) (production license no. SCXK20190003). A bank of two UVB lamps (Shenzhen Peninsula Medical Co., Ltd., China) was used as the UVB source (311 nm) and was placed above the back of each animal. The dorsal skin was irradiated with a dose of 120 mJ cm⁻² d⁻¹ for the first 2 days and a dose of 100 mJ cm⁻² d⁻¹ for the subsequent 3 days.

Twenty mice were divided into four groups: (1) the negative control (NC) group, in which the mice did not undergo UVB irradiation; (2) the UVB group, in which the mice underwent UVB irradiation every day; (3) the Aa group, in which the mice were treated Aa 10 mg kg⁻¹ before UVB irradiation; and (4) the TSRL group, in which the mice were treated with 100 mg kg⁻¹ TSRL protein before UVB irradiation. The dorsal skin of each mouse was photographed and then collected. Part of the skin was fixed with 10% formalin for histopathological analysis, and the other part was used to detect the GSH, malondialdehyde (MDA), and superoxide dismutase (SOD) levels.

The tissues were then cleared in xylene, embedded in paraffin, and cut to a thickness of 4 μm. The sections were stained with hematoxylin and eosin (H&E) for epidermal hyperplasia analysis; Masson trichrome for collagen fiber analysis; and resorcin-fuchsin for elastic fiber arrangement analysis. The histopathological changes in of each group were observed using an optical microscope. The collagen fiber content was quantified with the image analysis program Image-Pro Plus 6.0.

3. Results and discussion

3.1. Discovery and production of an antioxidant protein from sea anemone adhesives

Antioxidant components should exist in sea anemone adhesives to maintain the redox balance of the sea anemone adhesion interface. The complex composition of adhesive proteins results in low-solubility of the collected materials for most sessile marine organisms, so extraction was applied to harvest footprint proteins of sea anemones [21]. As shown in Fig. 1, the SDS-PAGE observations suggested that the resulting extracts contained numerous components that were significantly different from those of scallop byssal extracts, although the footprints were washed thoroughly after being scraped off the pedal disk [16,22]. Since it is not possible to further filter out the unwanted ectodermal cellular proteins [23], the extracts were subjected to LC-MS/MS analysis. A total of 1262 proteins were identified. Precise identification of the pivotal footprint components remained challenging, so comparative transcriptomics was deemed necessary to further identify the adhesive proteins of sea anemones.

We hypothesized the key interface proteins would be significantly differentially expressed between the adhesive glands and the remaining body tissues. Therefore, comparative transcriptome analysis was performed to reveal the genetic information of the related glands [24]. Total RNA was separately extracted from the *Haliplanella luciae* pedal disc and remaining body tissues (Fig. 2), and then subjected to Illumina sequencing on the HiSeq 4000 platform. Table S1 summarizes the details for *de novo* assembly and output sequences. Based on the screening criteria, 402 out of 109069 unigenes exhibited significantly different expression in the pedal disc compared with the rest of the animal, among which 314 genes were upregulated. Among the upregulated genes, 32 genes were identified in the footprints (Supplementary File 1).

Based on the integrated multi-omics screening analysis, detailed protein sequence analysis was undertaken to further pinpoint the antioxidant proteins. 32 candidates were annotated and divided into several main categories, including tyrosinases, structural proteins related to the extracellular matrix (ECM), and hypothetical novel proteins (Supplementary File 1). As shown in Fig. 2, c69606_g2_i4 (identified as TSRL) exhibited elevated expression among the candidates, indicating that the

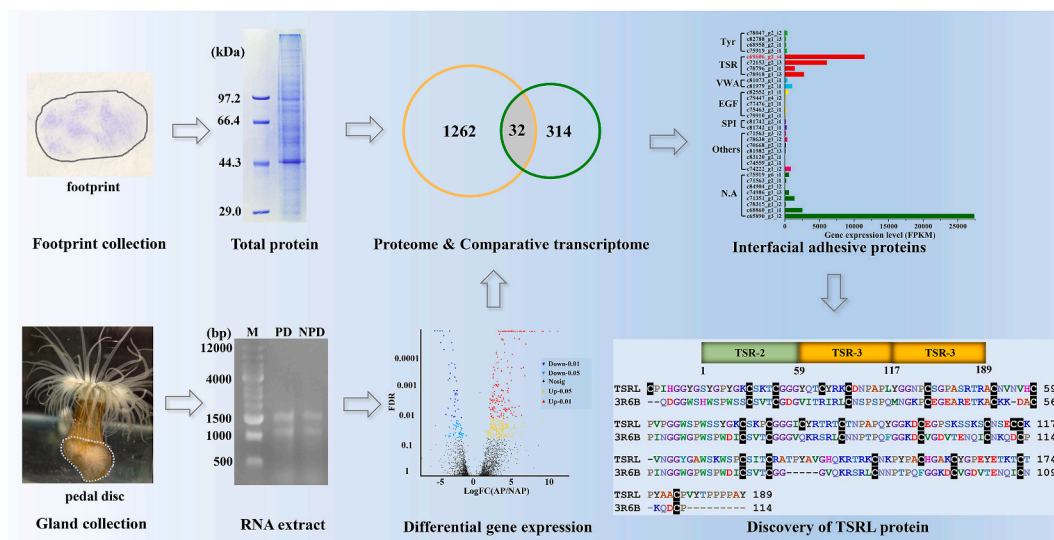


Fig. 2. Discovery of the TSRL protein from complicated sessile marine organism adhesives. SDS-PAGE exhibited multiple protein bands in footprints, suggesting the presence of unwanted ectodermal cellular proteins. In parallel, comparative transcriptome analysis identified 314 transcripts that were differentially upregulated in the pedal disc (PD: pedal disc; NPD: remaining body tissues). Among the upregulated genes, 32 were identified in the footprints. The bar graph of candidate expression levels in pedal discs shows that c69606_g2_i4 (named TSRL) exhibited elevated expression. The TSRL protein contained a high portion of cysteine residues (13%), which was hypothesized to endow the protein with antioxidant properties. Sequence alignment further showed that the TSRL protein had high sequence identity (46%) with an ECM component (3R6B, human TSR), indicating satisfactory biocompatibility for tissue regeneration.

TSRL protein was abundant in the sea anemone adhesives. Amino acid composition analysis showed a high proportion of cysteine residues (13%) in the TSRL protein, which might endow the protein with antioxidant properties [25]. Sequence alignment showed that the TSRL protein had high sequence identity (46%) with ECM components, suggesting satisfactory biocompatibility for tissue regeneration [26]. Overall, the TSRL protein was ultimately identified as an ideal candidate for antioxidant biomaterials through a combined strategy including interactive omics techniques and bioinformatics analysis. Since omics libraries have already been built for the adhesives of several sessile marine organisms, including barnacles, ascidians and limpets, this established strategy might facilitate the discovery of new functional biomaterials (Fig. 1).

Scaled-up production of pure TSRL protein was necessary for subsequent characterization and analysis of future applications. Direct extraction of the TSRL protein from sea anemone pedal discs was not feasible, so genetic engineering technology was applied to produce a high-purity recombinant TSRL protein. After optimization, a recombinant expression system was constructed using the pET vector and cultured in a large-scale bioreactor, and the protein was further purified in inclusion bodies (Fig. S1, Supporting Information). A yield of 500 mg L⁻¹ was achieved for recombinant TSRL with a purity of 80%. The efficient overexpression and purification procedure facilitated the following characterization and analysis of future applications.

3.2. TSRL-based wet-resistant coating with antioxidant activity

Mucus secreted from marine organisms can quickly self-assemble into firm cements or adhesives when exposed to seawater [27]. K⁺, Na⁺, Ca²⁺, Mg²⁺, Zn²⁺, and Fe³⁺ are abundant in seawater and play an important role in physiological conditions, so they were chosen to simulate the assembly behavior of the TSRL protein in marine environment [28]. Surprisingly, a TSRL-based reticular coating formed after the introduction of Ca²⁺ and Mg²⁺, whereas a more compact structure appeared on the glass slides after the introduction of Ca²⁺ alone (Fig. 3B). SEM was used to observe the ultrastructure of the coating after a layer of platinum film with a thickness of approximately 8 nm was sputtered onto it to increase the conductivity and resolution of the coating [29]. The microscopy images revealed that the Ca²⁺-induced meshwork structure was composed of homogenous spherical nanoparticles (Fig. 3C). The coatings were able to adhere to diverse surfaces, including glass, polystyrene and aluminium. In addition, the human TSR protein, a homologous protein of TSRL, did not react with Ca²⁺, which showed the uniqueness of the TSRL protein derived from sea anemones (Fig. 3D). The protein coatings remained stable after shaking in a humid environment for 48 h, showing exceptional water resistance and stability [30]. Water-resistant adhesives, sealants and coatings can avoid dramatic adhesion reduction in the presence of water or moisture. Thus, a sea anemone-inspired Ca²⁺-mediated protein coating with water-resistance might have excellent potential for use in clinical medicine (Fig. 3A).

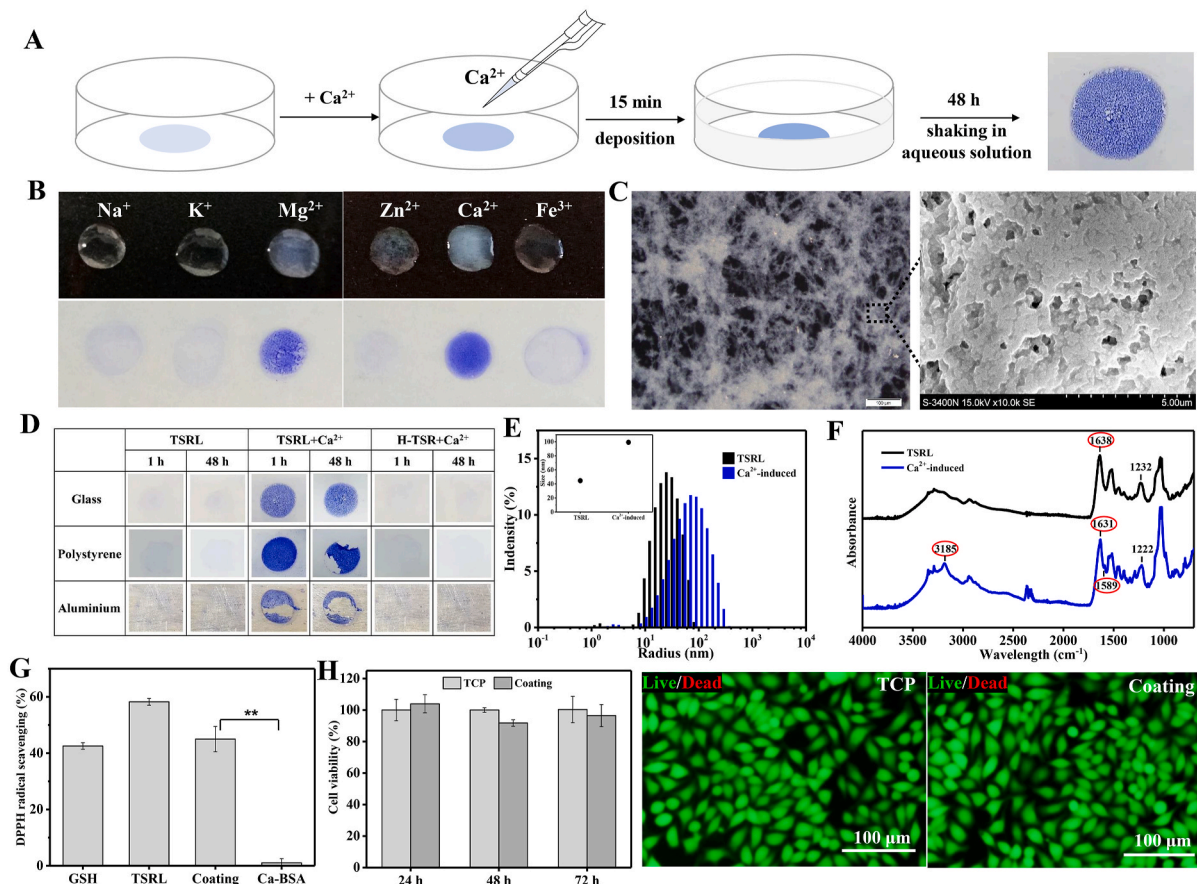


Fig. 3. The TSRL protein assembles into a wet-resistant coating with antioxidant activity. A) Diagram showing the formation of the TSRL-based coating. B) The self-assembly behavior of the TSRL protein (1 mg mL⁻¹) occurred in the presence of various metal ions (10 mM). C) Observation of the microstructure of the Ca²⁺-induced coating. Scale bar = 100 μm. D) Surface coating analysis suggested that the coating exhibited remarkable water resistance and stability on diverse substrates. H-TSR, human TSR. E) As measured by DLS, the protein particle size increased after incubation with Ca²⁺. F) The shift in the absorption peaks indicated the formation of cross-linking between Ca²⁺ and the TSRL protein. G) A DPPH radical scavenging assay of the coating showed antioxidant activity. H) Study on the cytocompatibility of the coating: cell viability and live/dead cell staining. Scale bar = 100 μm.

The assembly kinetics of diverse ion-binding proteins were characterized through turbidity measurements at 340 nm [31]. In the presence of divalent ions (Ca^{2+} , Mg^{2+} , Zn^{2+}) or Fe^{3+} , a distinct increase in turbidity was induced, while the addition of K^+ or Na^+ did not result in a significant change (Fig. S2, Supporting Information). Ca^{2+} induced the aggregation of the TSRL protein to form a regular network structure, but had no effect with human TSR protein (Figs. S3 and 4, Supporting Information). The Ca^{2+} -mediated self-assembly mechanism of TSRL-based coatings was then explored based on the DLS and FTIR results, which clarified the roles of Ca^{2+} in coating formation (Fig. 3E and F). After incubation with Ca^{2+} , the particle size of the proteins increased from 44 nm to 100 nm; this increase was accompanied by a peak shift of the amide I band from 1638 to 1631 cm^{-1} . The shift in absorption wavelength indicated the interaction of a calcium chelate and a carboxyl oxygen [32]. Two extra absorption peaks at 1589 and 3185 cm^{-1} appeared (N–H vibration band), showing that calcium-crosslinked bonds participated through interactions with amino nitrogen atoms [33]. These results indicated the formation of coordination bonds between Ca^{2+} and specific amino acids of the TSRL protein.

Radical scavenging and cytotoxicity assays were carried out to evaluate the antioxidant activity and biocompatibility of the naturally derived Ca^{2+} -mediated coating (Fig. 3G and H). The TSRL protein in solution scavenged 58% of DPPH free radicals within 30 min, while the coated TSRL protein scavenged 40% of DPPH free radicals; this difference was possibly due to conformational shifts caused by the Ca^{2+} that affected the free thiol activity. L929 cell viability was above 90% when the cells were cultured on the coating, indicating good

cytocompatibility. Metal ion-mediated biomaterials extensively exist in marine adhesives [34]. Recently, the sea star multimodular rSfp1 protein was assembled into valuable coatings with an irregular meshwork under $\text{Na}^+/\text{Ca}^{2+}$ conditions [35]. A variety of coatings have been designed with marine adhesive proteins [36], but no natural antioxidant biomaterial has been reported. The results obtained with our TSRL-based coating derived from sea anemones support the future application of marine antioxidant materials in pharmaceuticals and biomedicine.

3.3. TSRL-based hydrogels with tunable mechanical properties

The recombinant TSRL protein also self-assembled into hydrogels at suitable concentrations ($>30 \text{ mg mL}^{-1}$) (Fig. 4A). Hydrogel formation was accompanied by protein self-aggregation. Homogeneous nanoparticles with a size of $\sim 35 \text{ nm}$ appeared at low protein concentrations (Fig. 4B), while larger nanoparticles with a size of $\sim 570 \text{ nm}$ aggregated at higher concentrations after 48 h. DLS measurements revealed the uniformity and size distribution of the self-assembled protein aggregates during gelation (Fig. 4B). The TSRL protein in aqueous solution exhibited a homogeneous particle size distribution that was associated with the hydrodynamic diameter (D_h value). A gradual increase in D_h was observed over time, which confirmed the self-assembly behavior. FTIR spectra were then acquired to monitor protein conformation changes during hydrogel formation (Fig. 4C). Typical amide I, II and III absorption peaks at 1638 cm^{-1} , 1515 cm^{-1} and 1230 cm^{-1} remained for TSRL both in solution and in the hydrogel during the gelation process

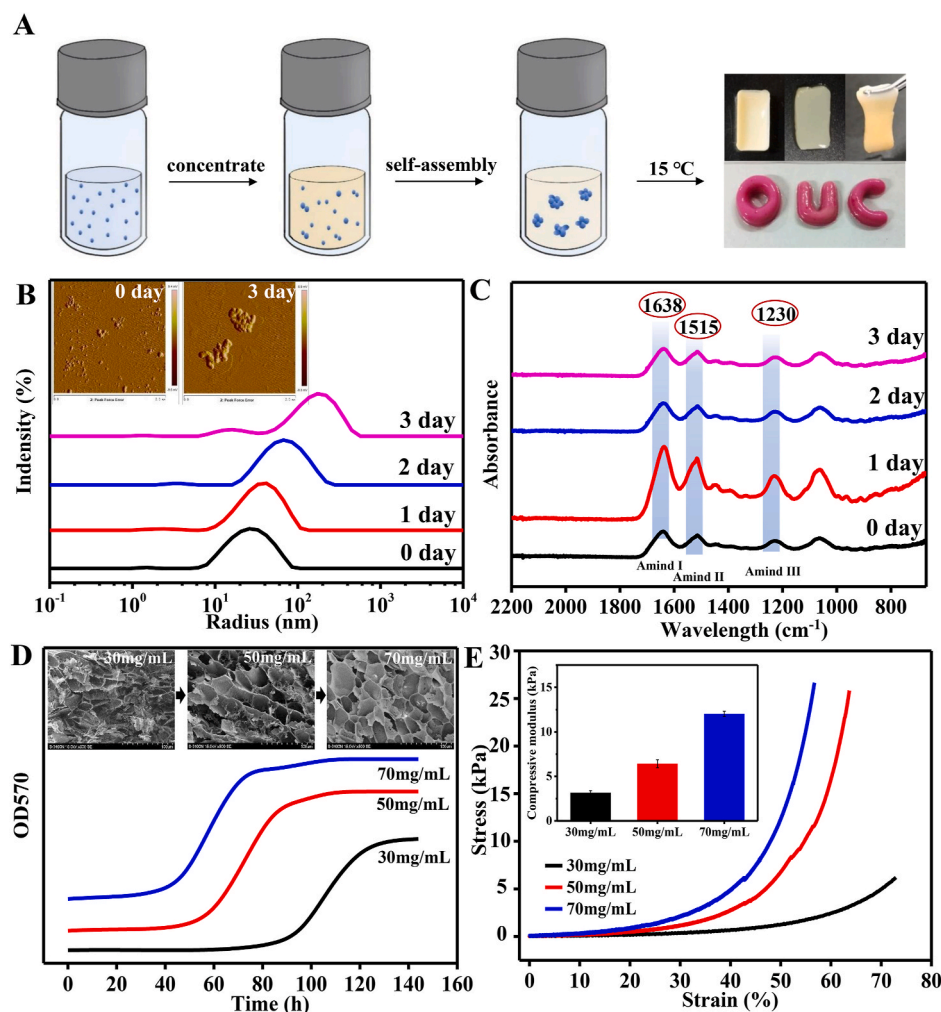


Fig. 4. The recombinant TSRL protein self-assembles into a versatile hydrogel. A) At a suitable concentration, the TSRL protein self-assembled into a hydrogel at 15 °C. B) The hydrodynamic diameter (D_h) value of the TSRL protein gradually increased during gelation, as detected by DLS measurements, and the protein particles increased in size from 35 to 570 nm according to AFM observation. Scale bar = 2 μm . C) The secondary structure remained unchanged during hydrogel formation according to FTIR. D) The turbidities of the TSRL protein solutions were monitored at 570 nm during gelation. Each data point is an average from five independent samples. SEM images of the lyophilized hydrogels with different concentrations are shown. Scale bar = 100 μm . E) The mechanical properties of the TSRL-based hydrogels were concentration-dependent. Error bars, standard deviation ($n = 4$).

[37–39]. The self-assembly of the TSRL protein was different from that of natural silk proteins, which often assemble into interconnected and branched nanofibers with beta-sheet structure formation [40,41].

The physical properties of TSRL-based hydrogels were investigated via optical, mechanical, and morphological approaches, and the results suggested that the gelation time, microstructure and mechanical properties were tunable concentrations from 30 to 70 mg mL⁻¹ (Fig. 4D and E). Sol-gel transformation occurred within 72 h at 70 mg mL⁻¹, while a longer gelation time was necessary at low concentrations. Correspondingly, the TSRL-based hydrogel with concentration of 30 mg mL⁻¹ failed to generate a regular network. Sponge-like scaffolds with a pore diameter of 36 μm began to appear until the concentration reached 70 mg mL⁻¹. With increasing protein concentrations, the compressive moduli of the hydrogels increased from 3.1 ± 0.3 to 12.0 ± 1.35 kPa, which is comparable to that of other native peptide-based hydrogels [42,43]. Additionally, physical properties, such as mechanical properties, regulate cell behaviors in tissue engineering [44]. Increasing the protein concentration in the sea anemone-inspired hydrogels increased their robustness and extensibility, supporting the usefulness of these hydrogels for regenerative medicine.

3.4. Redox-responsiveness of the TSRL-Based hydrogels

As mentioned above, the recombinant TSRL protein was rich in cysteine residues, which suggested that disulfide bonds may have played a critical role in hydrogel formation. DTT was added to disrupt disulfide bond formation, resulting in slower gelation (Fig. 5A). Previous studies have revealed that H₂O₂ can accelerate the formation of disulfide bonds [42]. To confirm the roles of the cysteine residues, H₂O₂ was added to the protein solution, and quicker gelation was observed (within 24 h). Similarly, redox-responsive microscale self-assembly was detected by DLS (Fig. 5B). The particle size in the H₂O₂-treated group (124 nm) was larger than that in the native group (63 nm), while the DTT-treated group showed a smaller hydrodynamic diameter (30 nm) after standing for 24 h. The H₂O₂-treated hydrogels showed a denser network structure than the native hydrogels, with a diameter of 10 μm, due to greater crosslinking of disulfide bonds. Hydrogel formation was able to be regulated under redox environmental conditions, which then influenced the mechanical properties, biodegradability, stability and ultrastructure of the hydrogels.

3.4.1. Biodegradability

In vitro enzymatic hydrolysis experiments were performed to evaluate the potential biodegradability of the formed hydrogels (Fig. 5C).

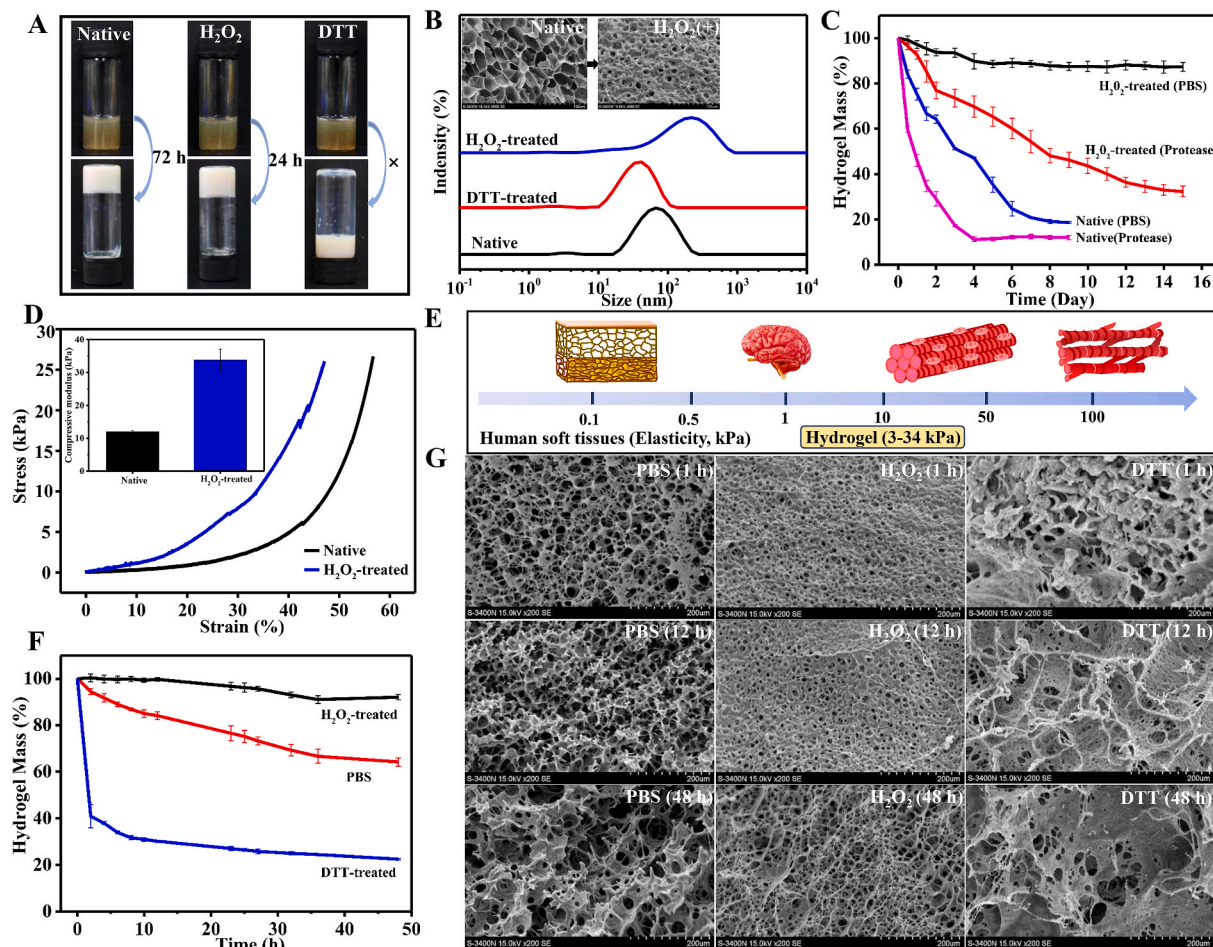


Fig. 5. Redox-responsiveness of the TSRL-based hydrogel. A) Influence of the redox environment (10 mM DTT or 0.03% H₂O₂) on the gelation process. B) Influence of redox conditions on the hydrodynamic diameter of the TSRL protein during hydrogel formation. The H₂O₂-treated hydrogels showed a denser microstructure than the native hydrogels according to SEM. Scale bar = 100 μm. C) *In vitro* biodegradation of native and H₂O₂-treated TSRL-based hydrogels. D) H₂O₂ treatment significantly improved the compressive modulus of the hydrogels. E) The elasticity of a range of human soft tissues (native fat, brain tissue, muscle tissue and myocardium) and comparison with the modulus achieved with TSRL-based hydrogels. F) The prepared hydrogels were incubated in PBS containing either H₂O₂ or DTT to investigate their stability under redox environments. G) The diverse surface morphology (porosity) of the hydrogels exposed to H₂O₂ or DTT was observed by SEM. Scale bar = 200 μm.

The hydrogels degraded significantly in PBS within 4 days. Only 20% of the original hydrogels remained after 10 days. The H₂O₂-treated group exhibited good stability with 87% weight retention within 15 days. Concurrently, the hydrogel weight of hydrogel was degraded by 68% after incubation with protease XIV within half a month, indicating good biodegradability of the TSRL-based hydrogels.

3.4.2. Mechanical properties

As shown in Fig. 5D, H₂O₂ treatment significantly improved the compressive modulus (33.8 ± 3.3 kPa). The mechanical properties of the hydrogels during enzymatic hydrolysis were further characterized. Interestingly, although the mass and volume of the TSRL-based hydrogels gradually decreased due to the discharge of water molecules from the network structure during enzymatic hydrolysis, however, the stiffness of remained hydrogels kept unchanged (Fig. S5, Supporting Information). The compressive modulus of H₂O₂-treated hydrogel reached 30 kPa after 5 days and 10 days. The tunable mechanical strength (3–34 kPa) of the hydrogels will likely facilitate their applications in various soft tissues such as native fat, brain tissue, muscle tissue, and the myocardium, which have different strengths in the range of 1–100 kPa [45–47] (Fig. 5E).

3.4.3. Stability

The disulfide bonds of proteins are affected by the redox environment, implying that biomaterials can be used for targeted drug release [48]. The TSRL-based hydrogels were incubated in PBS containing either H₂O₂ or DTT to investigate the potential redox-responsiveness. As shown in Fig. 5F, the hydrogels exhibited controllable degradation

kinetics. Hydrogels in PBS were relatively unstable and tended to degrade, losing 33% of their wet weight by 48 h. Quicker degradation was observed in a reducing environment, with only 25% of the wet weight remaining at 48 h. It is worth noting that the H₂O₂-treated hydrogel showed only 8% degradation, indicating better stability due to higher crosslinking via disulfide bonds.

3.4.4. Microstructure

SEM images of the hydrogels revealed that morphological changes occurred in the redox environment (Fig. 5G). After incubation in PBS, the pores of the newly formed hydrogels were slightly fused, with hole formation in the pore walls. The H₂O₂-treated hydrogels retained a constant regular porous structure over 48 h, suggesting minor degradation. Conversely, the DTT-treated hydrogels lost their shape or structural integrity within 1 h, indicating that the destruction of disulfide bonds led to the formation of heterogeneously distributed pores throughout the structure [49]. Redox-sensitive degradation is beneficial for biomaterials. For instance, these biomaterials could be used as sensors to detect oxidants or reductants, or as drug delivery systems to target the prevalent reductive intracellular environments of tumor cells [50].

3.5. Antioxidant properties of the TSRL-based hydrogel

In general, proteins containing amino acids with redox-sensitive side chain groups, such as Trp, Tyr, Cys, Met, and His, tend to exhibit antioxidant activity [1]. Thiol-derived biomaterials have been proven to have excellent antioxidant activity and are used in cardiac and neuronal

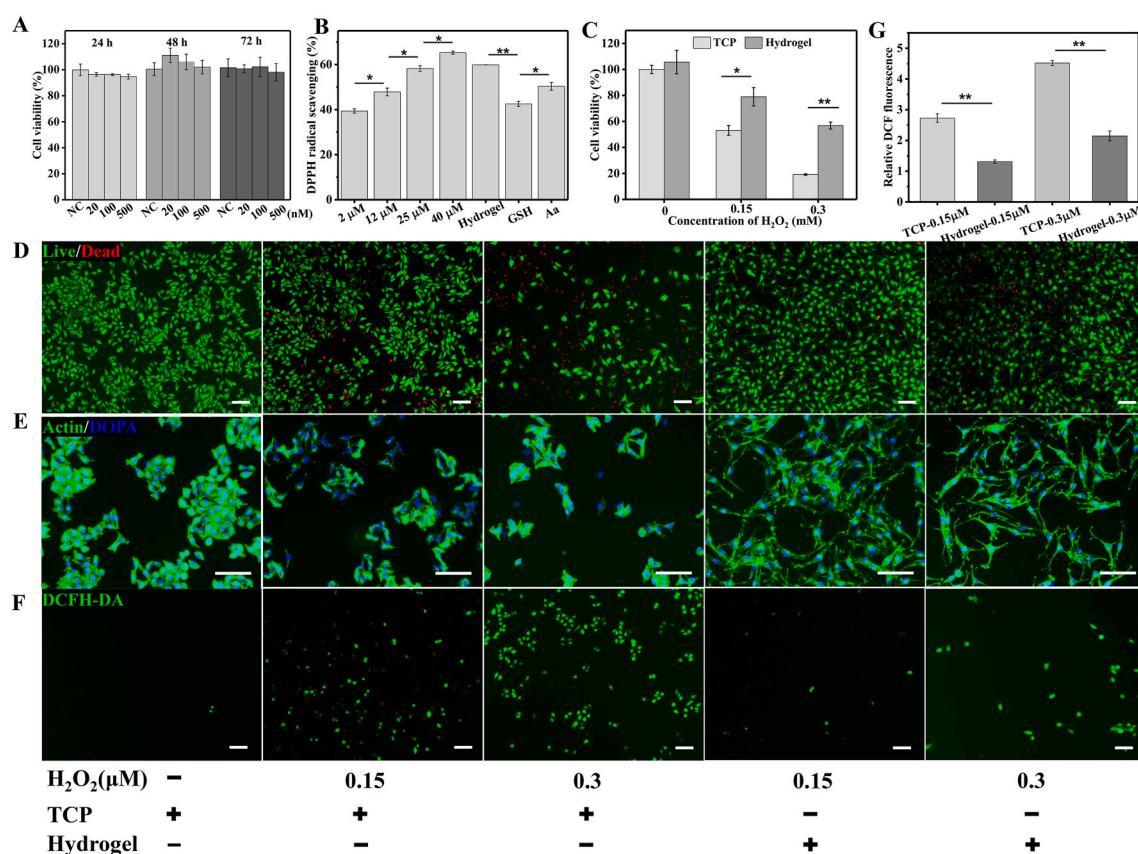


Fig. 6. Antioxidant activity of the TSRL-based hydrogels. A) Cell viability of L929 cells after 24, 48, and 72 h of culture with the TSRL protein. B) DPPH radical scavenging assay with the TSRL protein and TSRL-based hydrogels. C) Cell viability of L929 cells cultured on TCP or hydrogels after exposure to different doses of H₂O₂ (0, 0.15 and 0.3 mM). D) Representative images of live/dead cell staining after H₂O₂ treatment showing the survival statuses of cells after acute oxidative stress. E) Representative images of actin/DOPA staining after H₂O₂ treatment showing the morphological changes in of cells after acute oxidative damage. F) Effects of TSRL-based hydrogels on total intracellular ROS (DCFH-DA) in L929 cells after H₂O₂ treatment. Scale bar = 100 μm. G) Quantification of DCFH-DA staining. *p < 0.05, **p < 0.01, n = 3.

regeneration [2,51]. In this study, the antioxidant activity of the cysteine-rich TSRL protein was evaluated *in vitro* and *in vivo*.

MTT assays and F-actin staining were first performed to study the cytocompatibility of the hydrogels [52]. The cell viability was above 95% after culture on TSR protein at different concentrations (Fig. 6A). Significant increases in cell numbers occurred for all the groups after 48 h, suggesting the cytocompatibility of the hydrogels (Fig. S6, Supporting Information). Cells cultured on the TSRL-based hydrogel spread completely after 9 h, which indicated good adhesion of the cells on the hydrogels. In addition, we carried out the long-term cytotoxicity of the prepared hydrogel. It is known that the protein-based biomaterials generally demonstrated well biocompatibility, since they were degraded into small peptides or amino acids, that would promote cell adhesion and growth. As shown in Fig. S7 (Supporting Information), compared with the untreated group (NC), the hydrogel extracts had no obvious effect on cell activity after degradation in the protease XIV for 5 and 10 days. All the results suggested that the TSRL-based hydrogels had excellent biocompatibility and were candidate antioxidant biomaterials.

3.5.1. *In vitro* antioxidant experiments

The antioxidant activity of the TSRL-based hydrogel was monitored *in vitro* on the basis of the ability of the hydrogels to scavenge free radicals in solution and intracellular ROS. As shown in Fig. 6B, the ability to scavenge DPPH free radicals was dependent on the dose of the TSRL protein, increasing from 39% to 65% when the concentration increased from 2 μM to 40 μM . The TSRL protein demonstrated stronger antioxidant activity than the canonical small molecule antioxidants GSH and Aa, suggesting the promising future of TSRL-based proteins as antioxidant biomaterials.

H_2O_2 was then used to simulate the ROS produced by exogenous injury in L929 cells in order to assess the antioxidant capacity of the TSRL-based hydrogels (Fig. S8, Supporting Information) [53]. As shown in Fig. 6C, half of the cells survived when 0.15 mM H_2O_2 was introduced, but the hydrogel-treated cells retained 79% activity. The cell activity decreased to 19% in medium containing 0.3 mM H_2O_2 but was preserved at 57% when the hydrogel was present. The influence of the TSRL-based hydrogels on the survival and morphology of cells under oxidative stress was evaluated using a live/dead cell staining kit and Actin-Tracker Green (Fig. 6D and E). Compared with normal culture conditions, culture with H_2O_2 solution resulted in a large number of dead cells (red) in the control group. The distributions of the cytoplasm and nucleus were heterogeneous, indicating that apoptosis occurred [52]. When the cells were cultured on the hydrogels, almost all the cells remained alive, which was consistent with the results of the cell viability measurement. Thus, the TSRL-based protein hydrogels have an excellent ability to resist oxidative stress damage.

Next, the fluorescent dye DCFH-DA was used to evaluate the intracellular ROS content [54]. As shown in Fig. 6F, strong green fluorescence was observed in the control group, indicating the generation of intracellular ROS by the L929 cells exposed to the levels of H_2O_2 . The DCF fluorescence intensity in the hydrogel groups was significantly weaker than that in the tissue culture plate (TCP), indicating that the TSR-based hydrogels effectively suppressed the generation of intracellular ROS (Fig. 6G). These results suggested that the TSRL-based hydrogels markedly reduced ROS, which further reduced oxidative stress damage to the L929 cells.

The overexpression of ROS contributes to the pathogenesis of numerous diseases, such as atherosclerosis, myocardial infarction, and chronic inflammation. ROS-responsive biomaterials have emerged as a useful platform for regulating critical aspects of oxidative stress-induced exogenous pathologies [55,56]. As previously described, the elastic modulus of TSRL-based hydrogels meets the requirements of brain and muscle tissue (Fig. 5D). Therefore, hydrogels with enhanced antioxidant activity are expected to be applied to these damaged soft tissues to rapidly remove the ROS produced by the lesion.

3.5.2. *In vivo* antioxidant experiments

We further evaluated the antioxidant activity of the TSRL protein in C57BL/6J mice to assess the ability of TSRL-based biomaterials to eliminate ROS *in vivo* (Fig. S9, Supporting Information) [57]. Free radicals can be produced in the skin after ultraviolet irradiation, which in turn causes oxidative damage, such as skin reddening and epidermal hyperplasia [58]. As expected, UVB irradiation led to redness and peeling of the skin (Fig. 7A). Under the same irradiation, skin treated with Aa or TSRL protein exhibited no signs of swelling and sunburn, implying that oxidative damage was restrained. H&E staining and epidermal thickness analysis showed that UVB irradiation caused the epidermis to become thicker (33 μm –112 μm) than normal dorsal skin (Fig. 7B and C). The typical changes were attenuated by TSRL protein or Aa, resulting in an epidermal thickness similar to that of normal skin. These results suggested that the TSRL protein prevented UVB-induced swelling and epidermal hyperplasia. Masson trichrome and resorcin-fuchsin staining were performed to observe collagen and elastic fiber arrangement (Fig. 7D and E). UVB irradiation led to significant degradation and disordered arrangement of collagen fibers in the dermis, and abnormal aggregation and hyperplasia of elastic fibers. In the TSRL protein-treated skin, normal structures and distributions of collagen and elastic fibers were maintained after UVB irradiation. Taken together, the results indicated that the TSRL protein was able to prevent hyperplasia, degradation of collagen fibers and irregular aggregation of elastic fibers induced by UVB irradiation, confirming the antioxidant capacity of this protein *in vivo*.

The excessive ROS produced by long-term exposure to ultraviolet light disrupts the balance between oxidation and antioxidation in cells, leading to a state of oxidative stress [59]. The protective mechanism of the TSRL protein was elucidated by investigating the levels of several cellular oxidative stress indicators, including MDA, SOD, and GSH [53]. MDA, as a key lipid oxidation product, indirectly reflects the intracellular injury caused by oxidative stress. As shown in Fig. 7F, the MDA content was higher increased in the UVB group than in NC group, whereas the MDA content was lower in the TSRL group than in the UVB group, suggesting that lipid oxidation in mice skin was alleviated by TSRL protein treatment. The GSH and SOD levels decreased in the UVB group (Fig. 7G and H), but remained constant in the TSRL group, suggesting that the TSRL protein prevented UVB-induced cell damage by stimulating endogenous antioxidant systems including antioxidants and related enzymes. The TSRL protein not only exhibits free radical scavenging ability, but also self-assembles into different material forms, such as coating and hydrogel form, which suggests that TSRL-based biomaterials can scavenge ROS for acute oxidative stress (skin photoaging) prophylaxis and chronic oxidative stress (wound healing) cell therapies [51,60].

4. Conclusion

A combination of multi-omics techniques and genetic engineering, allowed us to efficiently screen a cysteine-rich antioxidant protein from among the 1262 adhesive components of sea anemones. The biocompatible TSRL protein not only retained expected antioxidant properties after scaled-up production, but also self-assembled into different forms of materials with beneficial properties. The formed TSRL-based coatings quickly adsorbed onto diverse surfaces and showed considerable stability in moist environments. The easy-to-use TSRL-based hydrogels exhibited tunable physical properties such as mechanical properties, micromorphology and stability upon exposure to the designed redox-stimuli. The TSRL-based hydrogels improved cell survival ability under oxidative stress, and prevented the oxidative damage caused by UVB irradiation. Therefore, this study provides an innovative platform to design biomaterials with desired bioactive properties, which will lead to new opportunities in biomimetics, biomedicines, and tissue engineering.

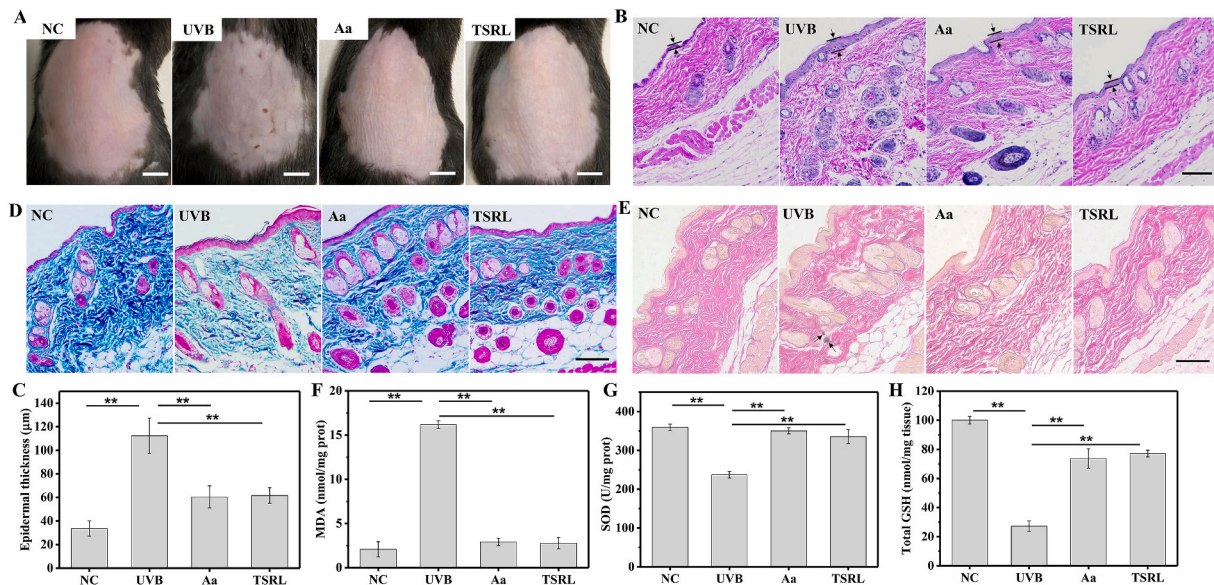


Fig. 7. Protective effects of the TSRL protein against UVB-induced oxidative damage. C57BL/6J mice were irradiated with UVB for five days, and animals were sacrificed 24 h after the last UVB exposure. A) Macroscopic changes observed, Scale bar = 5 mm. B) Dorsal skin was collected and fixed with 10% formalin. The representative H&E-stained sections show epidermal hyperplasia (100 \times). Scale bar = 100 μ m. C) The epidermal thicknesses of mouse skin was measured in each group (n = 5). D) Representative Masson trichrome staining for collagen fiber evaluation, Scale bar = 100 μ m. E) Representative resorcin-fuchsin staining for elastic fiber arrangement evaluation. The arrows mark abnormal aggregation and hyperplasia of elastic fibers. Scale bar = 100 μ m. F) MDA, G) SOD and H) GSH levels in mice skin with different treatments.

CRediT authorship contribution statement

Lulu Wang: Investigation, Formal analysis, Writing – original draft. **Xiaokang Zhang:** Investigation, Formal analysis, Validation. **Pingping Xu:** Writing – review & editing, Investigation. **Jicheng Yan:** Writing – review & editing, Investigation. **Yuzhong Zhang:** Formal analysis, Validation, Methodology, Visualization. **Hainan Su:** Investigation, Methodology. **Chengjun Sun:** Conceptualization. **Qiang Lu:** Funding acquisition, Resources, Project administration, Supervision, Writing – review & editing. **Weizhi Liu:** Funding acquisition, Resources, Project administration, Supervision, Writing – review & editing.

Declaration of competing interest

Prof. W. Liu and Dr. L. Wang are inventors on a patent application related to this work filed by Ocean university of China (No. CN 201910645175.0). The authors declare no conflict of interest.

Acknowledgments

The authors greatly appreciate Prof. Bo Dong (Ocean University of China) and Prof. Hai Xu (China University of Petroleum) for their technical guidance on this research. The authors gratefully acknowledge Shanghai Omicspace Biotechnology Co., Ltd. for technical assistance with peptide/protein identification. This work was supported by the Natural Science Foundation of China (32071371, 41776177), the Fundamental Research Funds for the Central Universities (201822024, 202061011), and the China Postdoctoral Science Foundation (2020M672143).

Appendix A. Supplementary data

Supplementary data to this article can be found online at <https://doi.org/10.1016/j.bioactmat.2021.08.021>.

References

- [1] I.S. Raja, N.N. Fathima, A gelatin based antioxidant enriched biomaterial by grafting and saturation: towards sustained drug delivery from antioxidant matrix, *Colloids Surf. B Biointerfaces* 128 (2015) 537–543.
- [2] A. Marino, C. Tonda-Turo, D. De Pasquale, F. Ruini, G. Genchi, S. Nitti, V. Cappello, M. Gemmi, V. Mattoli, G. Ciardelli, G. Ciofani, Gelatin/nanoceria nanocomposite fibers as antioxidant scaffolds for neuronal regeneration, *Biochim. Biophys. Acta Gen. Subj.* 1861 (2) (2017) 386–395.
- [3] Z. Xu, S. Han, Z. Gu, J. Wu, Advances and impact of antioxidant hydrogel in chronic wound healing, *Adv. Healthc. Mater.* 9 (5) (2020), e1901502.
- [4] C.R. Afonso, R.S. Hirano, A.L. Gaspar, E.G.L. Chagas, R.A. Carvalho, F.V. Silva, G. R. Leonardi, P.S. Lopes, C.F. Silva, C.M.P. Yoshida, Biodegradable antioxidant chitosan films useful as an anti-aging skin mask, *Int. J. Biol. Macromol.* 132 (2019) 1262–1273.
- [5] N. Khansari, Y. Shakiba, M. Mahmoudi, Chronic inflammation and oxidative stress as a major cause of age-related diseases and cancer, *Recent Pat. Inflamm. Allergy Drug Discov.* 3 (1) (2009) 73–80.
- [6] H. Kumar, K. Bhardwaj, E. Nepovimova, K. Kuća, D. Singh Dhanjal, S. Bhardwaj, S. K. Bhatia, R. Verma, D. Kumar, Antioxidant functionalized nanoparticles: a combat against oxidative stress, *Nanomaterials* 10 (7) (2020).
- [7] P.L. Thi, Y. Lee, D.L. Tran, T.T.H. Thi, J.I. Kang, K.M. Park, K.D. Park, In situ forming and reactive oxygen species-scavenging gelatin hydrogels for enhancing wound healing efficacy, *Acta Biomater.* 103 (2020) 142–152.
- [8] Q. Xu, C. He, C. Xiao, X. Chen, Reactive oxygen species (ROS) responsive polymers for biomedical applications, *Macromol. Biosci.* 16 (5) (2016) 635–646.
- [9] M.C. Wan, W. Qin, C. Lei, Q.H. Li, M. Meng, M. Fang, W. Song, J.H. Chen, F. Tay, L. N. Niu, Biomaterials from the sea: future building blocks for biomedical applications, *Bioact. Mater.* 6 (12) (2021) 4255–4285.
- [10] J. Yu, W. Wei, E. Danner, R.K. Ashley, J.N. Israelachvili, J.H. Waite, Mussel protein adhesion depends on interprotein thiol-mediated redox modulation, *Nat. Chem. Biol.* 7 (9) (2011) 588–590.
- [11] E. Valois, R. Mirshafian, J.H. Waite, Phase-dependent redox insulation in mussel adhesion, *Sci. Adv.* 6 (23) (2020), eaaz6486.
- [12] S.C. Nicklisch, S. Das, N.R. Martinez Rodriguez, J.H. Waite, J.N. Israelachvili, Antioxidant efficacy and adhesion rescue by a recombinant mussel foot protein-6, *Biotechnol. Prog.* 29 (6) (2013) 1587–1593.
- [13] D.R. Miller, J.E. Spahn, J.H. Waite, The staying power of adhesion-associated antioxidant activity in *Mytilus californianus*, *J. R. Soc. Interface* 12 (111) (2015), 20150614.
- [14] P.A. Davey, A.M. Power, R. Santos, P. Bertemes, P. Ladurner, P. Palmowski, J. Clarke, P. Flammang, B. Lengerer, E. Hennebert, U. Rothbacher, R. Pjeta, J. Wunderer, M. Zurovec, N. Aldred, Omics-based molecular analyses of adhesion by aquatic invertebrates, *Biol. Rev. Camb. Phil. Soc.* (2021).
- [15] P.A. Guerette, S. Hoon, Y. Seow, M. Raida, A. Masic, F.T. Wong, V.H. Ho, K. W. Kong, M.C. Demirel, A. Pena-Francesch, S. Amini, G.Z. Tay, D. Ding, A. Miserez, Accelerating the design of biomimetic materials by integrating RNA-seq with proteomics and materials science, *Nat. Biotechnol.* 31 (10) (2013) 908–915.

- [16] Y. Miao, L. Zhang, Y. Sun, W. Jiao, Y. Li, J. Sun, Y. Wang, S. Wang, Z. Bao, W. Liu, Integration of transcriptomic and proteomic approaches provides a core set of genes for understanding of scallop attachment, *Mar. Biotechnol.* 17 (5) (2015) 523–532.
- [17] E. Hennebert, B. Leroy, R. Wattiez, P. Ladurner, An integrated transcriptomic and proteomic analysis of sea star epidermal secretions identifies proteins involved in defense and adhesion, *J. Proteomics* 128 (2015) 83–91.
- [18] V. Kang, B. Lengerer, R. Wattiez, P. Flammang, Molecular insights into the powerful mucus-based adhesion of limpets (*Patella vulgata* L.), *Open Biol.* 10 (6) (2020), 200019.
- [19] S. Li, X. Huang, Y. Chen, X. Li, A. Zhan, Identification and characterization of proteins involved in stolon adhesion in the highly invasive fouling ascidian *Ciona robusta*, *Biochem. Biophys. Res. Commun.* 510 (1) (2019) 91–96.
- [20] L. Wang, L. Teng, X. Zhang, X. Liu, Q. Lyu, Y. Yang, W. Liu, Discovery and characterization of tyrosinases from sea anemone pedal disc, *J. Adhes. Sci. Technol.* 34 (17) (2020) 1840–1852.
- [21] E. Hennebert, B. Maldonado, P. Ladurner, P. Flammang, R. Santos, Experimental strategies for the identification and characterization of adhesive proteins in animals: a review, *Interface Focus* 5 (1) (2015) 20140064.
- [22] Y. Li, X. Sun, X. Hu, X. Xun, J. Zhang, X. Guo, W. Jiao, L. Zhang, W. Liu, J. Wang, J. Li, Y. Sun, Y. Miao, X. Zhang, T. Cheng, G. Xu, X. Fu, Y. Wang, X. Yu, X. Huang, W. Lu, J. Lv, C. Mu, D. Wang, X. Li, Y. Xia, Y. Li, Z. Yang, F. Wang, L. Zhang, Q. Xing, H. Dou, X. Ning, J. Dou, Y. Li, D. Kong, Y. Liu, Z. Jiang, R. Li, S. Wang, Z. Bao, Scallop genome reveals molecular adaptations to semi-sessile life and neurotoxins, *Nat. Commun.* 8 (1) (2017).
- [23] J.L. Clarke, P.A. Davey, N. Aldred, Sea anemones (*Exaiptasia pallida*) use a secreted adhesive and complex pedal disc morphology for surface attachment, *BMC Zoology* 5 (1) (2020).
- [24] D.G. DeMartini, J.M. Errico, S. Sjoestroem, A. Fenster, J.H. Waite, A cohort of new adhesive proteins identified from transcriptomic analysis of mussel foot glands, *J. R. Soc. Interface* 14 (131) (2017).
- [25] M. Huo, J. Yuan, L. Tao, Y. Wei, Redox-responsive polymers for drug delivery: from molecular design to applications, *Polym. Chem.* 5 (5) (2014) 1519–1528.
- [26] S.F. Badyalak, The extracellular matrix as a biologic scaffold material, *Biomaterials* 28 (25) (2007) 3587–3593.
- [27] M. Nakano, J.R. Shen, K. Kamino, Self-assembling peptide inspired by a barnacle underwater adhesive protein, *Biomacromolecules* 8 (6) (2007) 1830–1835.
- [28] C. Liu, L. Xie, R. Zhang, Ca^{2+} mediates the self-assembly of the foot proteins of *pinctada fucata* from the nanoscale to the microscale, *Biomacromolecules* 17 (10) (2016) 3347–3355.
- [29] B.H. Kemmenoe, G.R. Bullock, Structure analysis of sputter-coated and ion-beam sputter-coated films: a comparative study, *J. Microsc.* 132 (2) (1983) 153–163.
- [30] H. Qi, W. Zheng, C. Zhang, X. Zhou, L. Zhang, Novel mussel-inspired universal surface functionalization strategy: protein-based coating with residue-specific post-translational modification in vivo, *ACS Appl. Mater. Interfaces* 11 (13) (2019) 12846–12853.
- [31] M. Humenik, M. Magdeburg, T. Scheibel, Influence of repeat numbers on self-assembly rates of repetitive recombinant spider silk proteins, *J. Struct. Biol.* 186 (3) (2014) 431–437.
- [32] H. Hou, S. Wang, X. Zhu, Q. Li, Y. Fan, D. Cheng, B. Li, A novel calcium-binding peptide from Antarctic krill protein hydrolysates and identification of binding sites of calcium-peptide complex, *Food Chem.* 243 (2018) 389–395.
- [33] B. Yang, S. Jin, Y. Park, Y.M. Jung, H.J. Cha, Coacervation of interfacial adhesive proteins for initial mussel adhesion to a wet surface, *Small* 14 (52) (2018), e1803377.
- [34] S. Kim, H.Y. Yoo, J. Huang, Y. Lee, S. Park, Y. Park, S. Jin, Y.M. Jung, H. Zeng, D. S. Hwang, Y. Jho, Salt triggers the simple coacervation of an underwater adhesive when cations meet aromatic pi electrons in seawater, *ACS Nano* 11 (7) (2017) 6764–6772.
- [35] M. Lefevre, P. Flammang, A.S. Aranko, M.B. Linder, T. Scheibel, M. Humenik, M. Leclercq, M. Surin, L. Tafforeau, R. Wattiez, P. Leclere, E. Hennebert, Sea star-inspired recombinant adhesive proteins self-assemble and adsorb on surfaces in aqueous environments to form cytocompatible coatings, *Acta Biomater.* 112 (2020) 62–74.
- [36] H. Qi, C. Zhang, H. Guo, W. Zheng, J. Yang, X. Zhou, L. Zhang, Bioinspired multifunctional protein coating for antifogging, self-cleaning, and antimicrobial properties, *ACS Appl. Mater. Interfaces* 11 (27) (2019) 24504–24511.
- [37] K. Deepankumar, C. Lim, I. Polte, B. Zappone, C. Labate, M.P. De Santo, H. Mohanram, A. Palaniappan, D.S. Hwang, A. Miserez, Supramolecular β -sheet suckerin-based underwater adhesives, *Adv. Funct. Mater.* 30 (16) (2020).
- [38] L.-B. Jiang, D.-H. Su, S.-L. Ding, Q.-C. Zhang, Z.-F. Li, F.-C. Chen, W. Ding, S.-T. Zhang, J. Dong, Salt-assisted toughening of protein hydrogel with controlled degradation for bone regeneration, *Adv. Funct. Mater.* 29 (2019) 1901314.
- [39] J. Sirichaisit, V.L. Brookes, R.J. Young, F. Vollrath, Analysis of structure/property relationships in silkworm (*Bombyx mori*) and spider dragline (*Nephila edulis*) silks using Raman spectroscopy, *Biomacromolecules* 4 (2) (2003) 387–394.
- [40] A. Matsumoto, J. Chen, A.L. Collette, U.J. Kim, G.H. Altman, P. Cebe, D.L. Kaplan, Mechanisms of silk fibroin sol-gel transitions, *J. Phys. Chem. B* 110 (2006) 21630–21638.
- [41] S. Bai, X. Zhang, Q. Lu, W. Sheng, L. Liu, B. Dong, D.L. Kaplan, H. Zhu, Reversible hydrogel-solution system of silk with high beta-sheet content, *Biomacromolecules* 15 (8) (2014) 3044–3051.
- [42] M.L. Zhou, Z.G. Qian, L. Chen, D.L. Kaplan, X.X. Xia, Rationally designed redox-sensitive protein hydrogels with tunable mechanical properties, *Biomacromolecules* 17 (11) (2016) 3508–3515.
- [43] K. Schacht, T. Scheibel, Controlled hydrogel formation of a recombinant spider silk protein, *Biomacromolecules* 12 (7) (2011) 2488–2495.
- [44] N. Annabi, J.W. Nichol, X. Zhong, C. Ji, S. Koshy, A. Khademhosseini, F. Dehghani, Controlling the porosity and microarchitecture of hydrogels for tissue engineering, *Tissue Eng. B Rev.* 16 (4) (2010) 371–383.
- [45] C.B. Li, R. Martin, M. Seu, C. Zhang, Z. Zhou, J.S. Choi, X. Jiang, L. Chen, G. Walia, J. Yan, M. Callanan, H. Liu, K. Colbert, J. Morrisette-McAlmon, W. Grayson, S. Reddy, J.M. Sacks, H.Q. Mao, Nanofiber-hydrogel composite-mediated angiogenesis for soft tissue reconstruction, *Sci. Transl. Med.* 11 (2019), eaau6210.
- [46] J.T.S. Pettikiriarachchi, C.L. Parish, M.S. Shoichet, J.S. Forsythe, D.R. Nisbet, Biomaterials for brain tissue engineering, *Aust. J. Chem.* 63 (8) (2010).
- [47] C. Xu, W. Lee, G. Dai, Y. Hong, Highly elastic biodegradable single-network hydrogel for cell printing, *ACS Appl. Mater. Interfaces* 10 (12) (2018) 9969–9979.
- [48] H.B. Bingol, S. Agopcan-Cinar, T. Bal, D.C. Oran, S. Kizilel, N. Kayaman-Apohan, D. Avci, Stimuli-responsive poly(hydroxyethyl methacrylate) hydrogels from carboxylic acid-functionalized crosslinkers, *J. Biomed. Mater. Res.* 107 (9) (2019) 2013–2025.
- [49] Z. Gao, B. Golland, G. Tronci, P.D. Thornton, A redox-responsive hyaluronic acid-based hydrogel for chronic wound management, *J. Mater. Chem. B* 7 (47) (2019) 7494–7501.
- [50] R.S. Su, R.J. Galas Jr., C.Y. Lin, J.C. Liu, Redox-responsive resilin-like hydrogels for tissue engineering and drug delivery applications, *Macromol. Biosci.* 19 (8) (2019), e1900122.
- [51] T. Hao, J. Li, F. Yao, D. Dong, Y. Wang, B. Yang, C. Wang, Injectable fullerene/algininate hydrogel for suppression of oxidative stress damage in Brown adipose-derived stem cells and cardiac repair, *ACS Nano* 11 (6) (2017) 5474–5488.
- [52] S. Zhang, Q. Ou, P. Xin, Q. Yuan, Y. Wang, J. Wu, Polydopamine/puerarin nanoparticle-incorporated hybrid hydrogels for enhanced wound healing, *Biomater. Sci.* 7 (10) (2019) 4230–4236.
- [53] S. Zhang, J. Hou, Q. Yuan, P. Xin, H. Cheng, Z. Gu, J. Wu, Arginine derivatives assist dopamine-hyaluronic acid hybrid hydrogels to have enhanced antioxidant activity for wound healing, *Chem. Eng. J.* (2020) 392.
- [54] S.M. Farooq, N.B. Boppana, A. Devarajan, S.D. Sekaran, E.M. Shankar, C. Li, K. Gopal, S.A. Bakar, H.S. Karthik, A.S. Ebrahim, C-phycocyanin confers protection against oxalate-mediated oxidative stress and mitochondrial dysfunctions in MDCK cells, *PLoS One* 9 (4) (2014), e93056.
- [55] Q. Xu, M. Venet, W. Wang, J. Creagh-Flynn, X. Wang, X. Li, Y. Gao, D. Zhou, M. Zeng, I. Lara-Saez, S. A. H. Tai, W. Wang, Versatile hyperbranched poly(beta-hydrazide ester) macromers as injectable Antioxidative hydrogels, *ACS Appl. Mater. Interfaces* 10 (46) (2018) 39494–39504.
- [56] E. Ginter, V. Simko, V. Panakova, Antioxidants in health and disease, *Bratisl. Lek. Listy* 115 (10) (2014) 603–606.
- [57] D.N. Che, G.H. Xie, B.O. Cho, J.Y. Shin, H.J. Kang, S.I. Jang, Protective effects of grape stem extract against UVB-induced damage in C57BL mice skin, *J. Photochem. Photobiol., B* 173 (2017) 551–559.
- [58] B.O. Cho, D.N. Che, J.Y. Shin, H.J. Kang, J.H. Kim, H.Y. Kim, W.G. Cho, S.I. Jang, Ameliorative effects of *Diospyros lotus* leaf extract against UVB-induced skin damage in BALB/c mice, *Biomed. Pharmacother.* 95 (2017) 264–274.
- [59] Y. Liu, X. Huang, P. Wang, Y. Pan, D. Cao, C. Liu, A. Chen, The effects of HSP27 against UVB-induced photoaging in rat skin, *Biochem. Biophys. Res. Commun.* 512 (3) (2019) 435–440.
- [60] A.L. Lakes, C.T. Jordan, P. Gupta, D.A. Puleo, J.Z. Hilt, T.D. Dziubla, Reducible disulfide poly(beta-amino ester) hydrogels for antioxidant delivery, *Acta Biomater.* 68 (2018) 178–189.